SUPPORTING INFORMATION

Highly Efficient Synthesis of Microporous Zeolitic Imidazolate Framework-8 in Dimethyl Carbonate under Ambient Conditions

Alessandra Sessa,[a,1] Sara Vllahu, [a,1] Prisco Prete, [a] Ida Ritacco, [a] Laura Falivene,[a] Alessia Carbone, [a] Giovanni Pierri, [a] Federico Rossi, [b] Istvan Lagzi, [c,d] Maria Bastianini, [e] Raffaele Cucciniello [a,*]

[a] Department of Chemistry and Biology "Adolfo Zambelli", University of Salerno, viale Giovanni Paolo II 132, 84084 Fisciano (SA), Italy.

[b] Department of Physical Sciences, Earth and Environment, University of Siena, piazzetta Enzo Tiezzi 1, 53100 Siena, Italy.

[c] Department of Physics, Institute of Physics, Budapest University of Technology and Economics, Műegyetem rkp. 3, H-1111 Budapest, Hungary

[d] HUN-REN–BME Condensed Matter Physics Research Group, Budapest University of Technology and Economics, Műegyetem rkp. 3, H-1111 Budapest, Hungary

[e] R&D Department, Prolabin&Tefarm S.r.l., 06134 Ponte Felcino - Perugia, Italy

[1] These authors contributed equally to this manuscript.

INDEX

S1. Chemicals

Zinc acetate dihydrate (>99%, $Zn(CH_3COO)_2{\cdot}2H_2O$, CAS: 5870-45-6), 2-methylimidazole (99%, $C_4H_6N_2$, CAS: 693-98-1), sodium hydroxide (>98%, NaOH, CAS: 1310-73-2), dimethyl carbonate (99%, $C_3H_6O_3$, CAS: 616-38-6), methanol (CH_3OH, CAS: 67-56-1), chloroform-d (>99%, $CDCl_3$, CAS: 865-49-6) were purchased from Sigma Aldrich and used without further purification. Dimethyl carbonate/methanol mixtures with DMC/MeOH 1:2 and 2:1 molar composition were prepared by mixing the appropriate volumes of the two solvents. The 1:1 DMC/MeOH molar mixture was directly obtained as a by-product during the synthesis of glycerol carbonate (GlyC) through transcarbonatation of glycerol with dimethyl carbonate, as detailed in our previous work.[1] Table S1 summarizes the main properties of the solvents used in the solvothermal preparation of ZIF-8.

Table S1. Comparison of the main properties of solvents used for ZIF-8 synthesis, including traditional solvents (DMF, MeOH, H_2O) and alternative carbonate-based systems (GlyC and DMC).

Solvent	Boiling point at 1 atm (°C)	Dielectric constant at 20°C (ε)	Dipole moment (D)	Viscosity (mPa·s at 25°C)	Density (g cm^{-3} at 25°C)
DMF[2]	153	36.7	3.8	0.82	0.945
MeOH[2]	64	32.6	1.7	0.6	0.792
H_2O[2]	100	79.7	1.87	0.89	0.998
glyC[3,4]	110 (0.1 mmHg)	111.5	5.05	85.4	1.40
DMC[5]	90.3	3.1	0.91	0.585	1.07

S2. Synthesis and characterization of ZIF-8 samples

In this study, the Zn^{2+}: 2-methylimidazolate (2-mIM) molar ratio was initially set, considering the reaction stoichiometry, to 1:2. For each experiment, two separate starting solutions were prepared by dissolving a proper amount of each reagent precursor ($Zn(CH_3COO)_2{\cdot}2H_2O$ and 2-mIM in the same amount of the selected solvent, either DMC or a specific DMC/MeOH mixture, in order to

obtain the final concentrations reported in Table S2. Dissolution was favored by sonicating the solutions at room temperature for 1 minute. After that, the two precursors' solutions were combined in a one-necked glass flask, followed by the addition of a few µL of a 4 M NaOH aqueous solution. Each reaction was conducted for 1 hour at two different temperatures, namely room temperature and 60 °C, using a heating plate with a magnetic stirrer. All experimental procedures were performed under air and without any reagent/solvent pretreatment.

As a representative example (see entry 7 in Table S2), 0.1098g of zinc acetate dihydrate and 0.0821g of 2-mIM were dissolved separately in 50mL of the 2:1 DMC/MeOH molar mixture, corresponding to a final concentration of 5 mM and 10mM in 100 mL, respectively. The two solutions were then combined, and 250 µL of a 4 M NaOH aqueous solution was added to reach a final NaOH concentration of 10 mM in the reaction mixture.

The as-obtained precipitate was allowed to settle and cool down for 10 minutes, and the generated particles were collected by centrifugation at 4000 rpm for 5 minutes. After the removal of the mother liquor, the precipitates were subsequently rinsed with 5 mL of methanol to remove any unreacted species or by-products. For each sample, three washings were carried out, and then the purified product was dried in an oven at 80 °C for 12 hours. The isolated solid products were weighed after drying, and the corresponding reaction yields were calculated using the equation reported below:

$$Yield(\%) = \frac{experimental\ obtained\ mass\ ZIF-8\ (g)}{theoretic\ mass\ ZIF-8\ (g)} \times 100$$

The full set of reaction conditions tested in this study is summarized in Table S2.

Table S2. ZIF-8 experimental synthesis conditions.

Entry	$[Zn^{2+}]$ (mM)	[2-mIm] (mM)	C_{NAOH} (mM)	Solvent	*V* (mL)	*T* (°C)	*t* (h)
1	20	40	10	DMC/MeOH (2:1)	50	60	1
2	20	40	10	DMC/MeOH (2:1)	50	RT	1
3	10	20	10	DMC/MeOH (2:1)	50	60	1
4	10	20	10	DMC/MeOH (2:1)	50	RT	1
5	10	20	20	DMC/MeOH (2:1)	50	60	1
6	10	20	20	DMC/MeOH (2:1)	50	RT	1
7	5	10	10	DMC/MeOH (2:1)	100	60	1
8	5	10	10	DMC/MeOH (2:1)	100	RT	1
9	5	10	10	DMC/MeOH (1:1)	100	60	1
10	5	10	10	DMC/MeOH (1:1)	100	RT	1
11	5	10	10	DMC/MeOH (1:2)	100	60	1
12	5	10	10	DMC/MeOH (1:2)	100	RT	1
13	10	20	20	DMC	50	60	1
14	10	20	20	DMC	50	RT	1
15	5	10	10	DMC	100	60	1
16	5	10	10	DMC	100	RT	1

Each ZIF-8 sample was stored in powder form for characterizations and gas adsorption tests.

Characterization details

The synthesis of ZIF-8 was confirmed using X-ray powder diffraction (XRPD) measurements, the specific surface area and pore size distribution were provided by the nitrogen adsorption/desorption isotherm data evaluated via Brunauer-Emmet-Teller (BET) and Non-Local Density Functional Theory (NLDFT) methods, respectively, and the thermal stability was investigated by thermogravimetric analysis (TGA).

In detail, the XRPD diffractograms were collected using a Bruker D2 PHASER X-ray powder diffractometer at room temperature. The measurements were conducted using a standard CuKα beam (λ = 1.5418 Å) as a radiation source, at 30 kV accelerating voltage and 10mA current. The scans were carried out on as-synthetized samples in 2θ range of 5-40° with a step size of 0.016° in 2θ and an acquisition step-time of 2.6 s. Data was processed with Origin Pro 2018 software.

N_2 adsorption-desorption measurements were performed on a Quantachrome NOVA 4200e instrument using nitrogen gas at 77K. Prior to analysis, samples (20 mg) were outgassed under vacuum at 150 °C for 1h. BET specific surface areas were calculated from the adsorption branch in the relative pressure range from 0.003 to 0.05. For a direct comparison with literature data, BET-derived SSA were reported for all samples. The NLDFT equilibrium model was used for the determination of the pore size distribution (PSD), over the full relative pressure range (P/P_0 = 0.00-1.00). The total pore volume was derived from the amount of nitrogen adsorbed at P/P_0 =0.99, corresponding to the cumulative pore volume.

TGA data were recorded using a TA instrument, TGA Q500 V20.13 series. All samples were held in alumina pans and heated over a temperature range from 25 °C to 800 °C, with a heating rate of 10 °C min^{-1}, under a continuous flow of nitrogen gas.

The morphology of the samples was investigated with a FEG LEO 1525 scanning electron microscope (FE-SEM). FE-SEM micrographs were collected after depositing the samples on a stub and sputter coating with chromium for 20 seconds.

S3. NMR characterization of the DMC/MeOH waste mixture

NMR spectra of solvents were performed in $CDCl_3$ at room temperature on a Bruker Avance-400 MHz spectrometer (^1H: 400.13; ^{13}C: 100.61). The resonances are reported in ppm (δ). Spectra recording was performed using Bruker TopSpin v2.1 software. Data processing was performed using TopSpin v4.1.4 software.

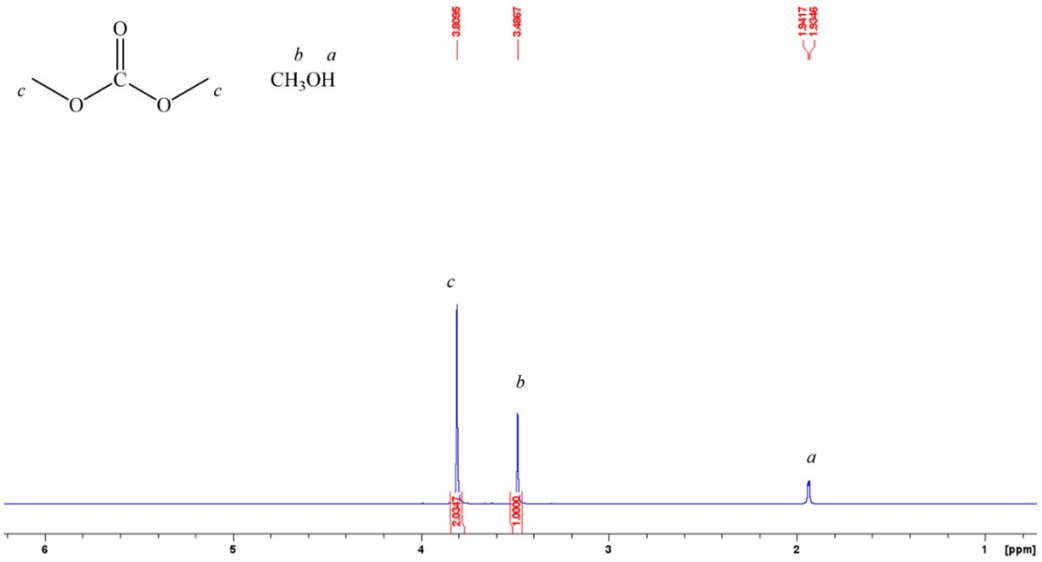

Figure S1. ^1H NMR of DMC/MeOH 1:1 mixture

^1H NMR (400MHz, $CDCl_3$, 298K), δ: 1.94 (*Ha*); 3.49 (s,3H;*Hb*); 3.80 (s,6H;*Hc*).

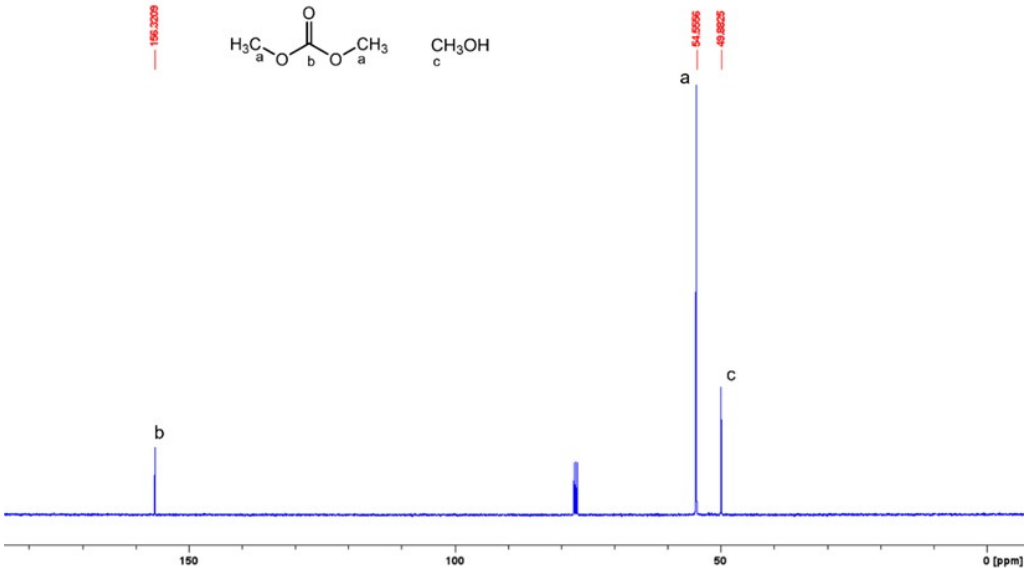

Figure S2. ^{13}C NMR of DMC/MeOH 1:1 mixture

^{13}C NMR (400MHz, $CDCl_3$, 298K), δ: 49.88 (*Cc*); 54.55 (2C; *Ca*); 156.32 (*Cb*).

S4. ZIF-8 characterizations

S4.1 ZIF-8 synthesis in DMC/MeOH 2:1

All the preliminary experiments in the DMC/MeOH 2:1 molar mixture are reported in Table S3, along with the corresponding reaction yields, specific surface area and pore volume values.

Table S3. Characterization of ZIF-8 synthesized in DMC/MeOH 2:1.

Entry	ZIF-8 formation[a]	Yield (%)	BET SSA ($m^2\ g^{-1}$)	Total pore volume ($cc\ g^{-1}$)
1	✓	51.1	1580	0.60
2	✗	-	-	-
3	✓	41.8	1235	0.63
4	✗	-	-	-
5	✓	97.2	770	0.32
6	✗	-	-	-
7	✓	97.5	921	0.38
8	✓	86.2	1350	0.51

[a] Confirmed by XRPD analysis
Reaction conditions are reported in Table S2.

XRPD analysis shown in Figure S3 confirmed the formation of the characteristic sodalite-type structure for each sample, with reflections at 2θ values of 7.3°, 10.4°, 12.7°, 14.7°, 16.4°, and 18.0°, corresponding to the (110), (200), (211), (220), (310), and (222) crystallographic planes.[6]

All BET isotherms shown in Figure S4 exhibited a Type I shape according to the IUPAC classification, a typical behavior for microporous materials. The initial rise in nitrogen adsorption corresponds to the filling of micropores (< 2 nm) in the ZIF-8 structure. The PSD, in the insert, showed a narrow and sharp peak centered around 0.616 nm half pore width, which is consistent with the expected ZIF-8 pore size.[7]

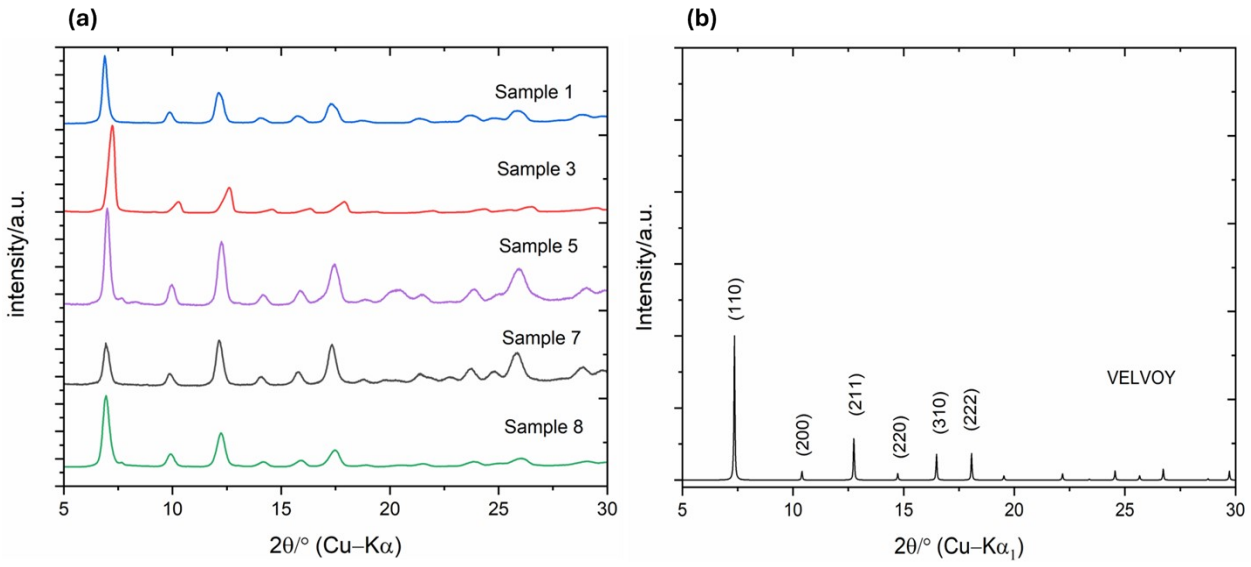

Figure S3. XRPD diffraction patterns of a) the synthesized samples (entries 1, 3, 5, 7 and 8), compared with b) the simulated ZIF-8 pattern (CCDC code VELVOY).

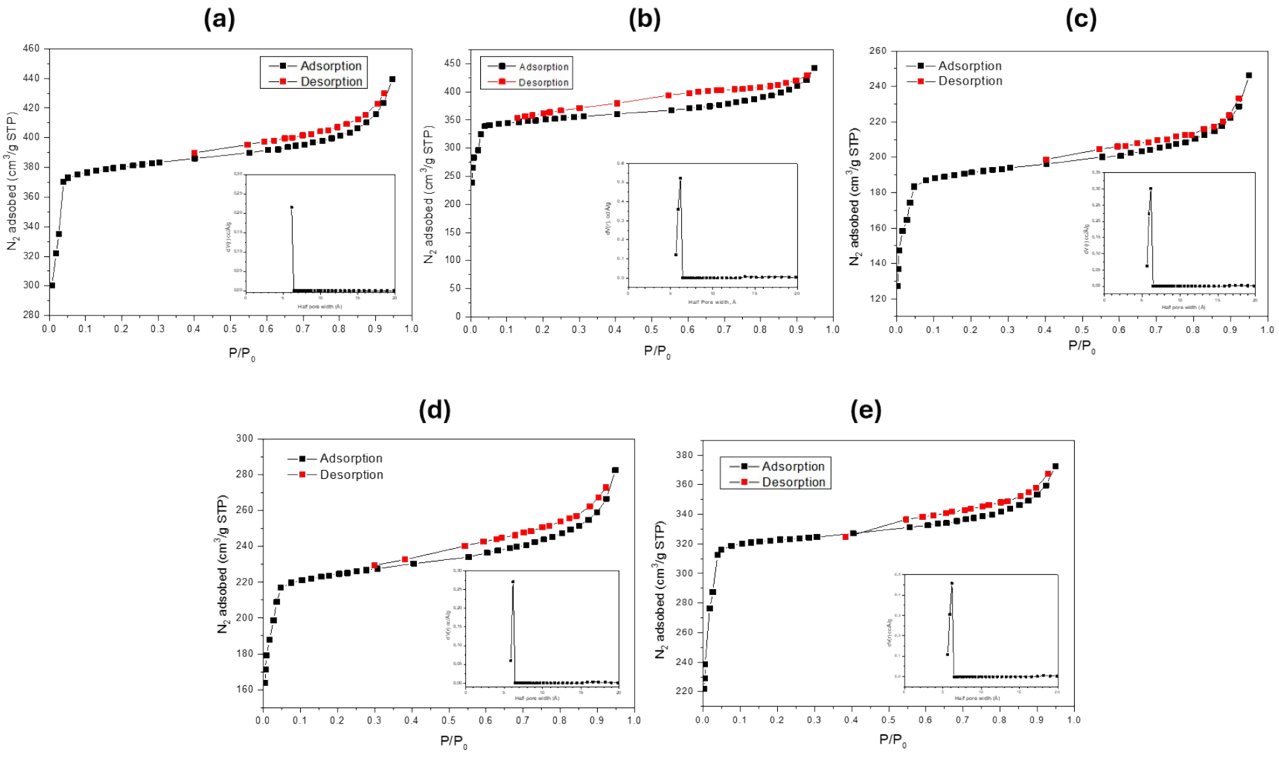

Figure S4. N_2 adsorption/desorption isotherm and PSD curves of ZIF-8 a) sample 1, b) sample 3, c) sample 5, d) sample 7, e) sample 8.

S4.2 ZIF-8 synthesis in DMC/MeOH 1:1

All the experiments carried out in the DMC/MeOH 1:1 molar mixture are reported in Table S4, along with the corresponding reaction yields, specific surface area and pore volume values.

Table S4. Characterization of ZIF-8 synthesized in DMC/MeOH 1:1.

Entry	ZIF-8 formation[a]	Yield (%)	BET SSA ($m^2\ g^{-1}$)	Total pore volume ($cc\ g^{-1}$)
9		69.5	1147	0.51
10		-	-	-

[a] Confirmed by XRPD analysis
Reaction conditions are reported in Table S2.

S4.3 ZIF-8 synthesized in DMC/MeOH 1:2

All the experiments carried out in the DMC/MeOH 1:2 molar mixture are reported in Table S5, along with the corresponding reaction yields, specific surface area and pore volume values.

Table S5. Characterization of ZIF-8 synthesized in DMC/MeOH 1:2.

Entry	ZIF-8 formation[a]	Yield (%)	BET SSA ($m^2\ g^{-1}$)	Total pore volume ($cc\ g^{-1}$)
11		-	-	-
12		-	-	-

[a] Confirmed by XRPD analysis
Reaction conditions are reported in Table S2.

Neither of the two experiments resulted in ZIF-8 crystallization, as confirmed by XRPD analysis (Figure S5), where no ZIF-8 phase was observed for both samples. These results are consistent with the known behavior of methanol-rich systems, in which crystallization typically requires more demanding conditions (Zn/2-mIM 1:8 molar ratio, 24 h at RT or Zn/2-mIM 1:3 molar ratio, 15 h at 60 °C).[8,9]

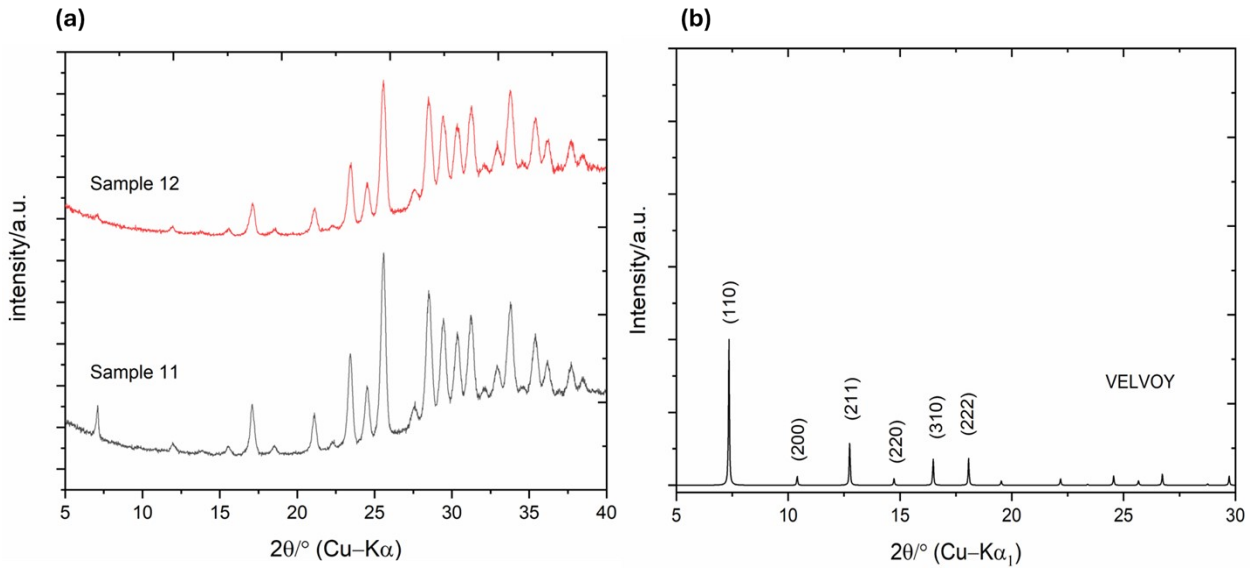

Figure S5. XRPD diffraction patterns of a) the synthesized samples (entries 11 and 12) compared with b) the simulated ZIF-8 pattern (CCDC code VELVOY).

These results showed that the mild conditions employed in this study are not suitable for this specific solvent mixture composition. However, this mixture was not further explored in the present work, since MeOH-based systems have already been widely studied in the literature, making this composition of lower interest in the context of developing alternative routes for ZIF-8 synthesis.

S4.4 ZIF-8 synthesis in DMC

All the experiments carried-out in pure DMC are reported in Table S6, along with the corresponding reaction yields, specific surface area and pore volume values.

Table S6. Characterization of ZIF-8 synthesized in pure DMC.

Entry	ZIF-8 formation[a]	Yield (%)	BET SSA ($m^2\ g^{-1}$)	Total pore volume ($cc\ g^{-1}$)
13	✗	-	-	-
14	✗	-	-	-
15	✗	-	-	-
16	✓	91.3	1522	0.75

[a] Confirmed by XRPD analysis. Reaction conditions are reported in Table S2.

S5. Stability of ZIF-8 samples

S5.1 Structural stability overtime: XRPD after 60 days

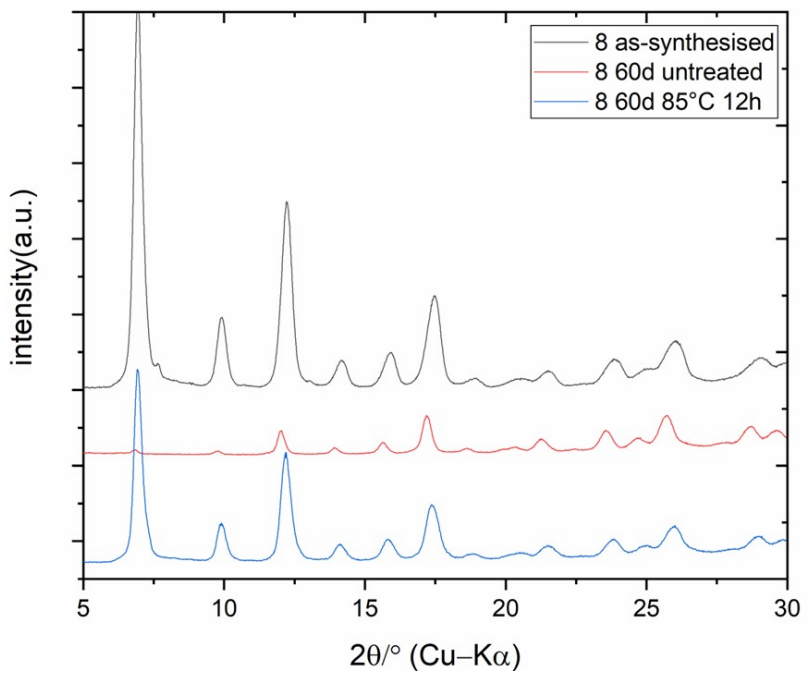

Figure S6. XRPD diffraction pattern of a ZIF-8 representative sample (sample 8) collected at different times: immediately after synthesis (black), after 60 days of storage at room temperature (red), and after 60 days followed by a thermal treatment at 85 °C for 12h (blue).

The XRPD pattern of ZIF-8 samples 8 is reported to evaluate its structural stability over time. The initial diffraction pattern (black) was obtained by performing the analysis on the as-synthesized powder samples, which were subsequently stored in glass vials at room temperature.

After 60 days from the synthesis, the sample was re-analyzed by XRPD both in its untreated state (red diffractogram) and after a thermal treatment in an oven at 85 °C for 12 hours (blue diffractogram). A comparative analysis of the red and blue spectra demonstrates that thermal treatment effectively reactivates the material, restoring all characteristic diffraction peaks. These results indicate that the synthesized ZIF-8 maintains its structural integrity over time under thermal activation conditions, without undergoing any degradation or requiring dry-state storage.

S5.1 Thermal stability: TG analysis

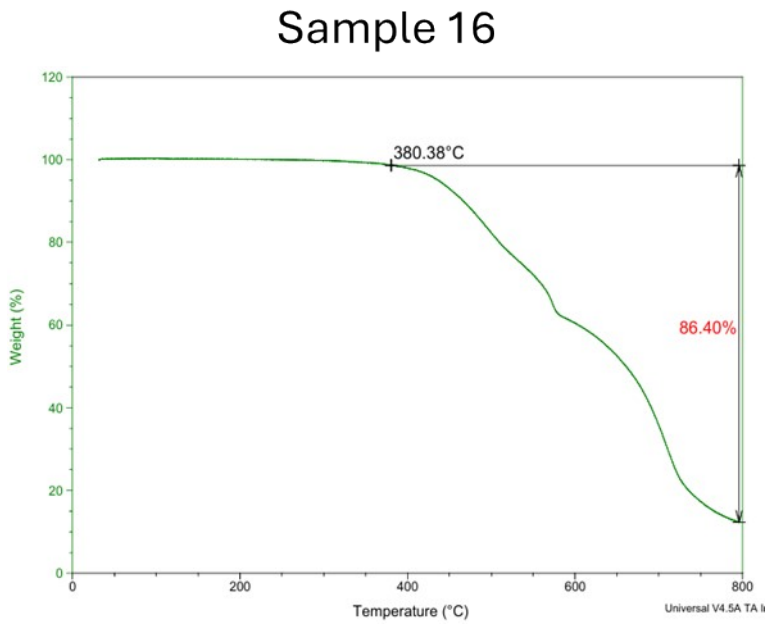

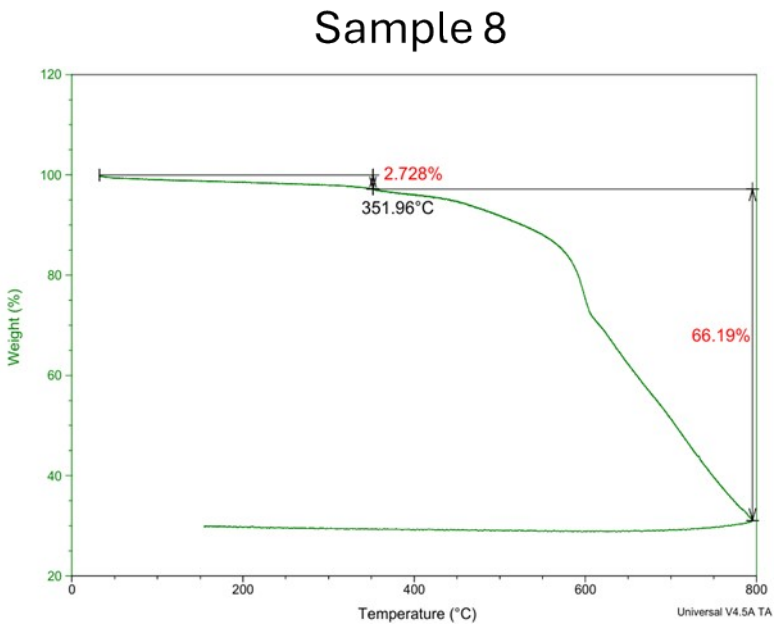

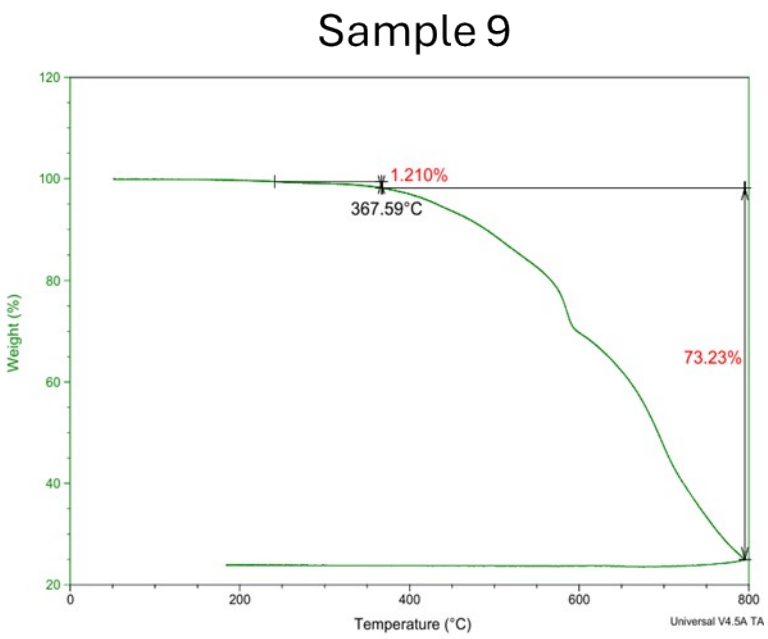

Figure S7. TGA scans of a representative ZIF-8 sample for each solvent/mixture employed for the synthesis.

S6. ZIF-8 in recycled DMC

In the solvent recycling experiments, after the first synthesis in fresh solvent (DMC), the mother liquor was recovered by centrifugation and filtered through a Nylon membrane filter (0.22 μm pore size) to remove suspended particles and aggregates. The filtered solvent was reused as reaction medium for a new ZIF-8 synthesis in an iterative procedure for two additional runs, using the same concentration of precursors and following the same procedure as the first synthesis conducted in fresh solvent.

In Figure S8 are shown ZIF-8 textural properties across all the synthesis cycles in recycled DMC.

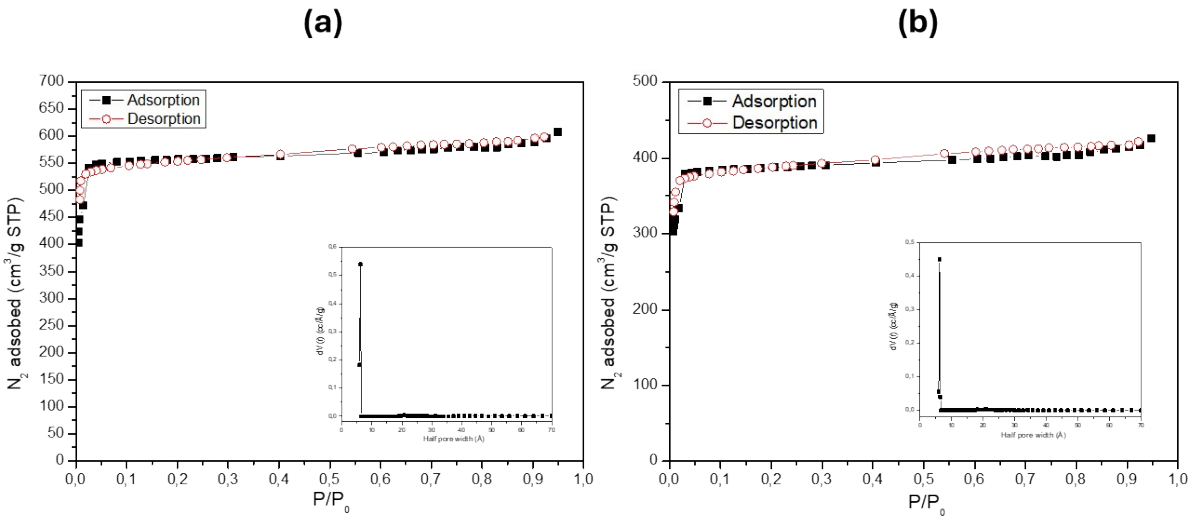

Figure S8. N_2 adsorption/desorption isotherm and pore size distribution (PSD) (insert) of ZIF-8 synthesized in recycled DMC (Samples a) 16-R_1, b) 16-R_2).

S7. Green metrics evaluation and LCA

S7.1 Green metrics

To evaluate the environmental impact of using DMC as an alternative solvent for ZIF-8 synthesis, green metrics like simple E-factor (sEF)[10] and Process Mass Intensity (PMI)[11] were calculated. These indicators quantify waste generation and overall mass efficiency for each synthesis. Additionally, PMI(r)[11] values were determined after each solvent recycling cycle.The obtained results were compared with literature data for ZIF-8 syntheses performed in DMF[12], H_2O[13], MeOH[9], and GlyC[1].

This study used the following equations:

Simple E-Factor (sEF):

$$sEF = \frac{\Sigma m(waste)}{\Sigma m(product)}$$

It quantifies the amount of waste generated per gram of product, excluding solvents and water.

Process Mass Intensity (PMI):

$$PMI = \frac{\Sigma m(materials\ in\ imput)}{\Sigma m(product)}$$

PMI measures the total input mass required per gram of product, including all reagents and solvents.

Process Mass Intensity after recycling (PMIr):

$$PMI(r) = \frac{\Sigma m(materials\ in\ imput) - m(recovered\ species)}{\Sigma m(product)}$$

PMIr considers material recycling within the process, giving a more sustainable perspective on resource efficiency.

S7.2 LCA

Software and database

The ecoinvent database (v.3.7.1)[14] was used for the background data, with "market for" scenarios selected to capture the impacts associated with average transportation distances. The market dataset includes all the activities related to a product within a specified region, including average transport and additional inputs to account for trade and transport losses. The following selection criteria were applied: given the international geographic context, priority was given to global providers ({GLO}), or European providers ({RER}) when {GLO} was unavailable. The Allocation at Point of Substitution (APOS, U) model was chosen, as it is considered the most conservative approach. This model allocates direct impacts based on physical flows, in contrast to other methodologies, such as consequential or cut-off approaches.

SimaPro software (v. 9.2.0.2)[15] served as the primary tool for the analysis. The harmonized life cycle impact assessment method ReCiPe 2016[16] was selected to assess potential environmental impacts. This method evaluates environmental effects across 18 categories at the midpoint, or "problem-oriented" level. The categories assessed include: Global Warming Potential (GWP), Stratospheric Ozone Depletion (SOD), Ionizing Radiation (IR), Ozone Formation, Human Health (OF_HH), Fine Particulate Matter Formation (FPMF), Ozone Formation, Terrestrial Ecosystems (OF_TE), Terrestrial Acidification (TA), Freshwater Eutrophication (FE), Marine Eutrophication (ME), Terrestrial Ecotoxicity (TET), Freshwater Ecotoxicity (FET), Marine Ecotoxicity (MET), Human Carcinogenic Toxicity (HCT), Human Non-Carcinogenic Toxicity (HNCT), Land Use (LU), Mineral Resource Scarcity (MRS), Fossil Resource Scarcity (FRS), and Water Consumption (WC). These categories can be further grouped into three endpoint-damage receptors: human health, ecosystems, and resource depletion. The endpoint method allows for the comparison of different processes based on a cumulative single score, which is here expressed in millipoints (mPt).

Scenarios depiction

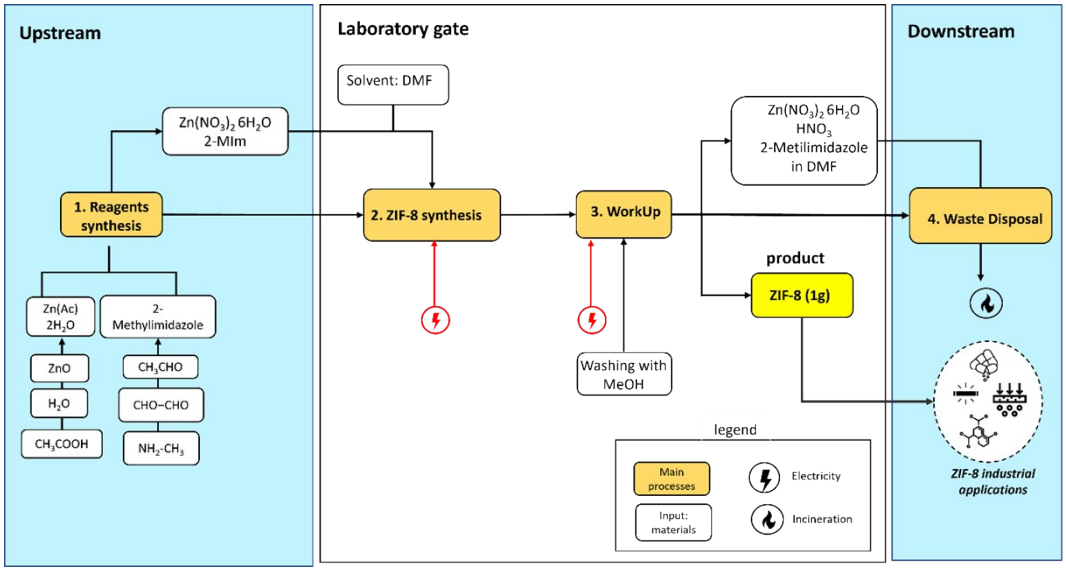

Figure S9. Flowchart for DMF-based scenario.

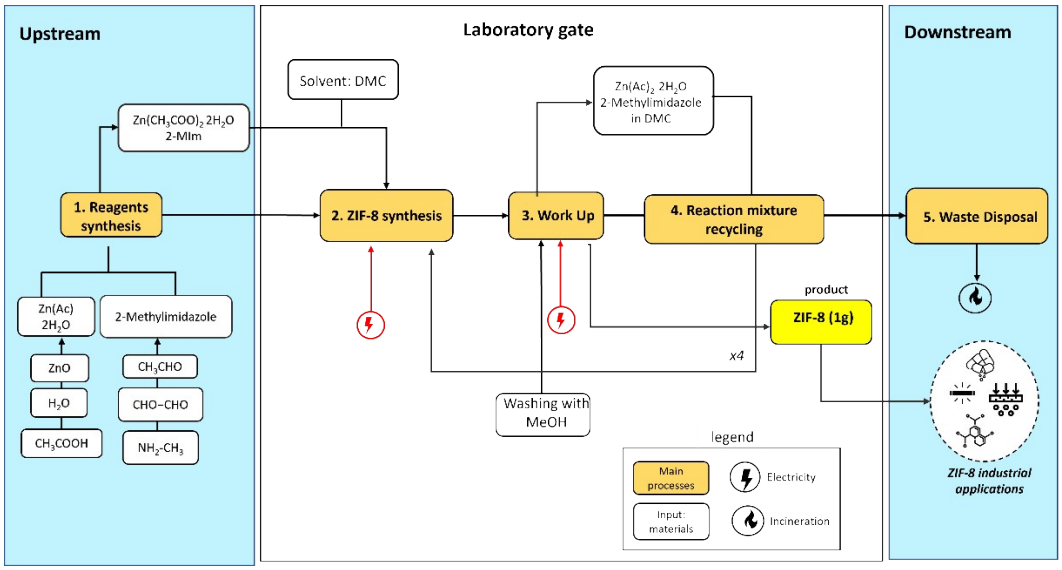

Figure S10. Flowchart for DMC-based scenario.

LCI (mass & energy inventory)

Table S7. LCI for DMF scenario

Item	Ecoinvent process	Type of process	Quantity	Unit of measurment
2-methylimidazole	_2-Methylimidazole*	INPUT	7.24	g
Zinc nitrate hexahydrate	*_zinc nitrate 6 H_2O**	INPUT	3.28	g
N,N-dimethylformamide (DMF)	*N, N-dimethylformamide {GLO} | market for | APOS, U*	INPUT	51	g
Electricity (ZIF-8 synthesis)	*Electricity, low voltage {GLO}| market group for | APOS, U*	INPUT	10.25	kWh
Electricity (Work-up)	*Electricity, low voltage {GLO}| market group for | APOS, U*	INPUT	3.23	kWh
Washing with MeOH	*Methanol {GLO}| market for | APOS, U*	INPUT	20	g
Waste to incineration	*spent solvent mixture {Europe without Switzerland} | treatment of spent solvent mixture, hazardous waste incineration, with energy recovery | APOS, U*	OUTPUT (waste)	60.39	g

Table S8. LCI for DMC scenario

Item	Ecoinvent process	Type of process	Quantity	Unit of measurment
2-methylimidazole	_2-Methylimidazole*	INPUT	0.83	g
Zinc acetate dihydrate	_zinc acetate $2H_2O$	INPUT	1.10	g
Dimethyl carbonate (DMC)	Dimethyl carbonate {GLO}| market for dimethyl carbonate | APOS, U	INPUT	303.88	g
Electricity (ZIF-8 synthesis)	*Electricity, low voltage {GLO}| market group for | APOS, U*	INPUT	3.94	kWh
Electricity (Work-up)	*Electricity, low voltage {GLO}| market group for | APOS, U*	INPUT	3.35	kWh
Washing with MeOH	*Methanol {GLO}| market for | APOS, U*	INPUT	70	g
Waste to incineration	*spent solvent mixture {Europe without Switzerland} | treatment of spent solvent mixture, hazardous waste incineration, with energy recovery | APOS, U*	OUTPUT (waste)	303.88	g

Energy consumption data sheet

For all calculations, standard laboratory instrument power has been considered. Also, the following models for the instrument are: Hermle Labortechnik(centrifuge), Heidolph -MR Hei-Standard (heating plate), Leroy Somer (vacuum pump), DERUI DR-MH60 (Ultrasonic cleaner), GLOBEINSTRUMENTS (Oven).

For temperature allocation: power and time of usage were multiplied by the factor $\Delta t/\Delta t_{max} = (T_{reaction}-T_{ext})/(T_{max}-T_{ext})$, where $T_{ext} = T_{laboratory} = 19°C$ ca.

Table S9. Laboratory equipment

Parameter	Heating Plate (Heidolph MR Hei-Standard)	Vacuum pump (Leroy Somer)	Centrifuge (Hermle Labortechnik)	Ultrasonic (DERUI DR-MH60)	Oven (GLOBE INSTRUMENTS)	Muffle (Nabertherm)
Power	0.825 kW	0.55 kW	0.58 kW	0.480 kW	0.750 kW	4.5 kW
Max Temperature (Tmax)	300 °C	-	-	-	300 °C	1000°C
Max Speed (Speedmax)	1400 rpm	-	13500	-	-	-

Table S10. Calculation setup for DMF scenario.

Parameter	ZIF-8 synthesis	Work Up ZIF-8
T reaction (°C)	140	120
Time	24 h	12 h
Energy	10.25	3.23

393

Parameter	ZIF-8 synthesis	Work up ZIF-8 centrifugation	Work Up ZIF-8 Oven)	Precursors' solutions
T reaction (°C)	RT	-	80	RT
Time	1 h	10+4 min	12 h	5-10 min
Speed	250 rpm	4000	-	-
ΔT/ΔTmax	-	-	0.062	-
Speed/Speed Max	0.18	0.30	-	-
Energy (kWh)	0.354	0.011	3.35	0.000263

394 **Table S11.** Calculation setup for DMC scenario.

395

396 **Table S12.** LCIA for DMF based scenario (MidPoint categories).

Impact category	Unit	2-MIM	$Zn(NO_3)_2$	DMF	Eletricity for mixing	Washing with MeOH	Exiccation	Incineration
Global warming	kg CO_2 eq	4.9E-02	6.4E-03	1.6E-01	7.7E+00	1.4E-02	2.4E+00	1.2E-01
Stratospheric ozone depletion	kg CFC11 eq	1.3E-08	1.1E-07	6.0E-08	3.2E-06	7.4E-09	1.0E-06	3.2E-08
Ionizing radiation	kBq Co-60eq	4.6E-03	1.2E-04	9.4E-03	9.3E-01	2.2E-04	2.9E-01	5.8E-04
Ozone formation, Human health	kg NOx eq	7.6E-05	9.4E-06	3.0E-04	1.7E-02	2.6E-05	5.3E-03	4.8E-05
Fine particulate matter formation	kg PM2.5 eq	4.8E-05	5.4E-06	2.1E-04	1.7E-02	1.3E-05	5.3E-03	2.0E-05
Ozone formation, Terrestrial ecosystems	kg NOx eq	7.7E-05	9.6E-06	3.0E-04	1.7E-02	2.6E-05	5.3E-03	4.8E-05
Terrestrial acidification	kg SO_2 eq	1.4E-04	2.0E-05	4.9E-04	2.6E-02	3.6E-05	8.1E-03	4.5E-05
Freshwater eutrophication	kg P eq	1.6E-05	9.4E-07	5.7E-05	3.8E-03	1.7E-06	1.2E-03	2.4E-05

Marine eutrophication	kg N eq	2.6E-05	7.2E-08	1.6E-04	2.8E-04	1.3E-07	8.8E-05	2.3E-06
Terrestrial ecotoxicity	kg 1,4-DCB	4.6E-03	8.6E-02	7.8E-02	5.6E+00	4.2E-04	1.8E+00	2.4E-03
Freshwater ecotoxicity	kg 1,4-DCB	6.1E-05	2.4E-04	3.6E-04	4.3E-01	1.3E-05	1.4E-01	3.3E-05
Marine ecotoxicity	kg 1,4-DCB	6.5E-05	3.8E-04	2.8E-04	5.5E-01	1.6E-05	1.7E-01	4.8E-05
Human carcinogenic toxicity	kg 1,4-DCB	4.9E-04	3.4E-04	2.4E-05	3.9E-01	3.7E-06	1.2E-01	1.9E-05
Human non-carcinogenic toxicity	kg 1,4-DCB	3.9E-04	8.9E-03	1.4E-03	6.5E+00	7.2E-05	2.1E+00	1.6E-04
Land use	m^2a crop eq	3.2E-03	2.4E-04	9.4E-03	3.2E-01	3.3E-04	1.0E-01	5.5E-04
Mineral resource scarcity	kg Cu eq	1.2E-04	1.9E-05	4.3E-04	7.8E-03	1.9E-05	2.5E-03	3.5E-05
Fossil resource scarcity	kg oil eq	2.6E-02	9.7E-04	8.1E-02	1.9E+00	1.5E-02	6.1E-01	3.9E-03
Water consumption	m^3	9.1E-04	4.4E-05	2.0E-03	6.1E-02	8.4E-05	1.9E-02	1.6E-04

Table S13. LCIA for DMC based scenario (MidPoint categories).

Impact category	**Unit**	**2-MIM**	**$Zn(AcO)_2$**	**DMC**	**Eletricity for mixing**	**Washing with MeOH**	**Exiccation**	**Incineration**
Global warming	kg CO_2 eq	5.56E-03	1.35E-03	6.86E-01	2.94E+00	4.87E-02	2.50E+00	6.00E-01
Stratospheric ozone depletion	kg CFC11 eq	1.47E-09	6.48E-10	1.82E-07	1.22E-06	2.57E-08	1.04E-06	1.59E-07
Ionizing radiation	kBq Co-60eq	5.28E-04	9.70E-05	4.91E-02	3.56E-01	7.81E-04	3.03E-01	2.93E-03
Ozone formation, Human health	kg NOx eq	8.67E-06	3.36E-06	1.43E-03	6.41E-03	9.03E-05	5.46E-03	2.41E-04
Fine particulate matter formation	kg PM2.5 eq	5.46E-06	2.19E-06	8.19E-04	6.43E-03	4.55E-05	5.47E-03	1.01E-04
Ozone formation, Terrestrial ecosystems	kg NOx eq	8.84E-06	3.55E-06	1.51E-03	6.47E-03	9.20E-05	5.50E-03	2.41E-04
Terrestrial acidification	kg SO_2 eq	1.64E-05	4.45E-06	1.78E-03	9.87E-03	1.25E-04	8.40E-03	2.24E-04
Freshwater eutrophication	kg P eq	1.83E-06	4.28E-07	2.06E-04	1.45E-03	5.78E-06	1.24E-03	1.22E-04

Marine eutrophication	kg N eq	3.01E-06	3.31E-08	1.88E-05	1.07E-04	4.61E-07	9.08E-05	1.15E-05
Terrestrial ecotoxicity	kg 1,4-DCB	5.29E-04	2.60E-02	6.12E-01	2.16E+00	1.49E-03	1.83E+00	1.19E-02
Freshwater ecotoxicity	kg 1,4-DCB	6.95E-06	7.97E-05	9.66E-04	1.67E-01	4.57E-05	1.42E-01	1.67E-04
Marine ecotoxicity	kg 1,4-DCB	7.46E-06	1.21E-04	1.26E-03	2.11E-01	5.55E-05	1.79E-01	2.43E-04
Human carcinogenic toxicity	kg 1,4-DCB	5.55E-05	1.22E-04	4.25E-04	1.51E-01	1.29E-05	1.29E-01	9.46E-05
Human non-carcinogenic toxicity	kg 1,4-DCB	4.45E-05	2.76E-03	8.22E-03	2.51E+00	2.52E-04	2.13E+00	8.27E-04
Land use	m^2a crop eq	3.71E-04	8.97E-05	4.53E-02	1.24E-01	1.14E-03	1.05E-01	2.74E-03
Mineral resource scarcity	kg Cu eq	1.39E-05	5.01E-06	2.50E-03	3.01E-03	6.54E-05	2.56E-03	1.77E-04
Fossil resource scarcity	kg oil eq	2.93E-03	7.05E-04	3.41E-01	7.39E-01	5.29E-02	6.29E-01	1.94E-02
Water consumption	m^3	1.04E-04	2.85E-05	6.65E-03	2.34E-02	2.96E-04	1.99E-02	8.06E-04

399

400 **Table S14.** LCIA for DMF based scenario (Endpoint categories).

Impact category	**Unit**	**2-MIM**	**$Zn(NO_3)_2$**	**DMF**	**Eletricity for mixing**	**Washing with MeOH**	**Exiccation**	**Incineration**
Total	mPts	1.70E+00	2.21E-01	6.01E+00	3.64E+02	4.52E-01	1.12E+02	2.26E+00
Human health	mPts	1.57E+00	2.12E-01	5.62E+00	3.52E+02	9.04E-03	1.08E+02	2.15E+00
Ecosystem	mPts	6.10E-02	7.55E-03	1.92E-01	9.79E+00	6.60E-06	3.00E+00	9.94E-02
Resources	mPts	6.60E-02	2.07E-03	1.95E-01	2.63E+00	1.26E-08	8.05E-01	1.02E-02

401

402

403 **Table S15.** LCIA for DMC based scenario (Endpoint categories).

Impact category	**Unit**	**2-MIM**	**$Zn(OAc)_2$**	**DMC**	**Eletricity for mixing**	**Washing with MeOH**	**Exiccation**	**Incineration**
Total	mPts	1.94E-01	6.57E-02	2.63E+01	1.36E+02	1.58E+00	1.16E+02	1.14E+01
Human health	mPts	1.80E-01	6.20E-02	2.46E+01	1.31E+02	1.40E+00	1.12E+02	1.08E+01
Ecosystem	mPts	6.96E-03	1.88E-03	8.49E-01	3.66E+00	5.11E-02	3.11E+00	5.00E-01
Resources	mPts	7.53E-03	1.75E-03	8.68E-01	9.81E-01	1.33E-01	8.35E-01	5.12E-02

S8. Computational details.

All geometries were optimized with Gaussian16 package[17] and the B3LYP-D3(BJ) level of theory[18,19] was used to optimize the geometries of all minima and transition states. For Zn the quasi relativistic LANL2DZ ECP effective core potential was employed[20] , whereas the 6-311G** basis set was used for the C, O, H, and N atoms. The reported free energies were obtained by adding gas-phase thermal corrections to the electronic energy in solvent (**polarizable continuum** model)[21] computed via single-point energy calculations in dimethyl carbonate (DMC) ($\varepsilon = 3.13$ at 25°C) by using the same computational protocol previously described for the gas-phase calculations. The optimized minima and transition states were verified by harmonic vibrational analysis to have no and one proper imaginary frequency, respectively.

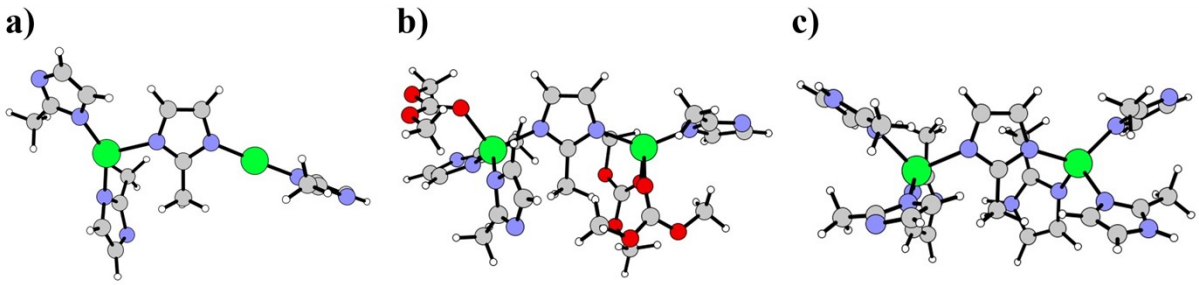

Figure S11. Optimized structures of a) $Zn_2(mIm)_4$, b) $Zn_2(mIm)_4(DMC)_3$ and c) $Zn_2(mIm)_4(Hmim)_3$. The Zn, C, O, H and N atoms are reported in green, silver, red, white, and blue and depicted in ball and stick.

S9. TEM analyses

Transmission electron microscopy (TEM) analysis was performed to investigate the morphology and size of the synthesized ZIF-8 particles. The samples were prepared by dispersing the powders in water and depositing 2 µL of the suspension onto a carbon-coated copper grid. The images were acquired using a FEI Tecnai microscope operating at an accelerating voltage of 120 kV.

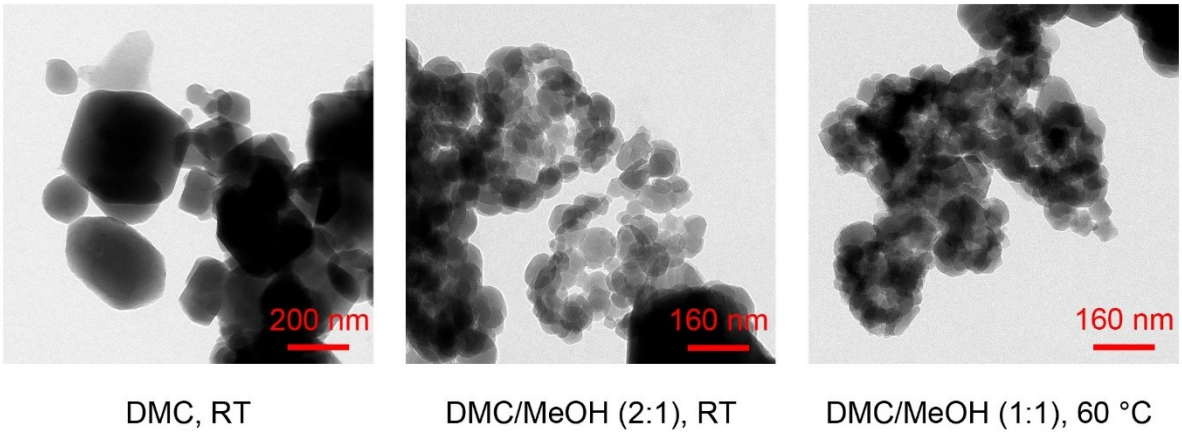

Figure S12. TEM micrographs of the ZIF-8 samples generated using different experimental conditions (solvent composition and temperature), keeping the reagents and base concentrations fixed: $[Zn^{2+}]$ = 5 mM, [Hmin] = 10 mM, and C_{NAOH} = 10 mM.

References

(1) Itatani, M.; Német, N.; Valletti, N.; Schuszter, G.; Prete, P.; Lo Nostro, P.; Cucciniello, R.; Rossi, F.; Lagzi, I. Synthesis of Zeolitic Imidazolate Framework-8 Using Glycerol Carbonate. *ACS Sustainable Chem. Eng.* **2023**, *11* (35), 13043–13049. https://doi.org/10.1021/acssuschemeng.3c02876.

(2) Smallwood, I. M. *Handbook of Organic Solvent Properties*; Halsted Pr. (Wiley): New York, 1996.

(3) Tatini, D.; Clemente, I.; Ambrosi, M.; Ristori, S.; Ninham, B. W.; Lo Nostro, P. Structuring Effect of Some Salts on Glycerol Carbonate: A near-Infrared Spectroscopy, Small- and Wide-Angle X-Ray Scattering Study. *Journal of Molecular Liquids* **2021**, *337*, 116413. https://doi.org/10.1016/j.molliq.2021.116413.

(4) Sonnati, M. O.; Amigoni, S.; Taffin De Givenchy, E. P.; Darmanin, T.; Choulet, O.; Guittard, F. Glycerol Carbonate as a Versatile Building Block for Tomorrow: Synthesis, Reactivity, Properties and Applications. *Green Chem.* **2013**, *15* (2), 283–306. https://doi.org/10.1039/C2GC36525A.

(5) Tundo, P.; Selva, M. The Chemistry of Dimethyl Carbonate. *Acc. Chem. Res.* **2002**, *35* (9), 706–716. https://doi.org/10.1021/ar010076f.

(6) Park, K. S.; Ni, Z.; Côté, A. P.; Choi, J. Y.; Huang, R.; Uribe-Romo, F. J.; Chae, H. K.; O'Keeffe, M.; Yaghi, O. M. Exceptional Chemical and Thermal Stability of Zeolitic Imidazolate Frameworks. *Proc. Natl. Acad. Sci. U.S.A.* **2006**, *103* (27), 10186–10191. https://doi.org/10.1073/pnas.0602439103.

(7) Russel, W. W. The Adsorption of Gases and Vapors. Volume I: Physical Adsorption (Brunauer, Stephen). *J. Chem. Educ.* **1944**, *21* (1), 52. https://doi.org/10.1021/ed021p52.1.

(8) Cravillon, J.; Münzer, S.; Lohmeier, S.-J.; Feldhoff, A.; Huber, K.; Wiebcke, M. Rapid Room-Temperature Synthesis and Characterization of Nanocrystals of a Prototypical Zeolitic Imidazolate Framework. *Chem. Mater.* **2009**, *21* (8), 1410–1412. https://doi.org/10.1021/cm900166h.

(9) Yang, X.; Song, T.; Su, T.; Hu, J.; Wu, S. Exploring the Influence of the Reused Methanol Solution for the Structure and Properties of the Synthesized ZIF-8. *Processes* **2022**, *10* (9), 1705. https://doi.org/10.3390/pr10091705.

(10) Sheldon, R. A. The E Factor at 30: A Passion for Pollution Prevention. *Green Chem.* **2023**, *25* (5), 1704–1728. https://doi.org/10.1039/D2GC04747K.

(11) Fantoni, T.; Tolomelli, A.; Cabri, W. A Translation of the Twelve Principles of Green Chemistry to Guide the Development of Cross-Coupling Reactions. *Catalysis Today* **2022**, *397–399*, 265–271. https://doi.org/10.1016/j.cattod.2021.09.022.

(12) Akhundzadeh Tezerjani, A.; Halladj, R.; Askari, S. Different View of Solvent Effect on the Synthesis Methods of Zeolitic Imidazolate Framework-8 to Tuning the Crystal Structure and Properties. *RSC Adv.* **2021**, *11* (32), 19914–19923. https://doi.org/10.1039/D1RA02856A.

(13) Kida, K.; Okita, M.; Fujita, K.; Tanaka, S.; Miyake, Y. Formation of High Crystalline ZIF-8 in an Aqueous Solution. *CrystEngComm* **2013**, *15* (9), 1794. https://doi.org/10.1039/c2ce26847g.
(14) Https://Ecoinvent.Org/ Accessed October 2025.
(15) Https://Simapro.Com/ Accessed October 2025.
(16) Huijbregts, M. A. J.; Steinmann, Z. J. N.; Elshout, P. M. F.; Stam, G.; Verones, F.; Vieira, M.; Zijp, M.; Hollander, A.; Van Zelm, R. ReCiPe2016: A Harmonised Life Cycle Impact Assessment Method at Midpoint and Endpoint Level. *Int J Life Cycle Assess* **2017**, *22* (2), 138–147. https://doi.org/10.1007/s11367-016-1246-y.
(17) Gaussian 16, Revision C.01, Frisch, M. J.; Trucks, G. W.; Schlegel, H. B.; Scuseria, G. E.; Robb, M. A.; Cheeseman, J. R.; Scalmani, G.; Barone, V.; Petersson, G. A.; Nakatsuji, H.; Li, X.; Caricato, M.; Marenich, A. V.; Bloino, J.; Janesko, B. G.; Gomperts, R.; Mennucci, B.; Hratchian, H. P.; Ortiz, J. V.; Izmaylov, A. F.; Sonnenberg, J. L.; Williams-Young, D.; Ding, F.; Lipparini, F.; Egidi, F.; Goings, J.; Peng, B.; Petrone, A.; Henderson, T.; Ranasinghe, D.; Zakrzewski, V. G.; Gao, J.; Rega, N.; Zheng, G.; Liang, W.; Hada, M.; Ehara, M.; Toyota, K.; Fukuda, R.; Hasegawa, J.; Ishida, M.; Nakajima, T.; Honda, Y.; Kitao, O.; Nakai, H.; Vreven, T.; Throssell, K.; Montgomery, J. A., Jr.; Peralta, J. E.; Ogliaro, F.; Bearpark, M. J.; Heyd, J. J.; Brothers, E. N.; Kudin, K. N.; Staroverov, V. N.; Keith, T. A.; Kobayashi, R.; Normand, J.; Raghavachari, K.; Rendell, A. P.; Burant, J. C.; Iyengar, S. S.; Tomasi, J.; Cossi, M.; Millam, J. M.; Klene, M.; Adamo, C.; Cammi, R.; Ochterski, J. W.; Martin, R. L.; Morokuma, K.; Farkas, O.; Foresman, J. B.; Fox, D. J. Gaussian, Inc., Wallingford CT, 2016.
(18) Allouche, A. Gabedit—A Graphical User Interface for Computational Chemistry Softwares. *J Comput Chem* **2011**, *32* (1), 174–182. https://doi.org/10.1002/jcc.21600.
(19) Grimme, S.; Antony, J.; Ehrlich, S.; Krieg, H. A Consistent and Accurate *Ab Initio* Parametrization of Density Functional Dispersion Correction (DFT-D) for the 94 Elements H-Pu. *The Journal of Chemical Physics* **2010**, *132* (15), 154104. https://doi.org/10.1063/1.3382344.
(20) Hay, P. J.; Wadt, W. R. *Ab Initio* Effective Core Potentials for Molecular Calculations. Potentials for K to Au Including the Outermost Core Orbitals. *The Journal of Chemical Physics* **1985**, *82* (1), 299–310. https://doi.org/10.1063/1.448975.
(21) Da Silva, C. O.; Mennucci, B. The Optical Rotation of Glucose Prototypes: A Local or a Global Property? *J. Chem. Theory Comput.* **2007**, *3* (1), 62–70. https://doi.org/10.1021/ct600250w.